ACS Photonics

pubs.acs.org/journal/apchd5

Letter

Single-Shot Real-Time Ultrafast Imaging of Femtosecond Laser Fabrication

Yunhua Yao,[#] Yilin He,[#] Dalong Qi,* Fengyan Cao, Jiali Yao, Pengpeng Ding, Chengzhi Jin, Xianyu Wu, Lianzhong Deng, Tianqing Jia, Feng Huang,* Jinyang Liang, Zhenrong Sun, and Shian Zhang*

Cite This: *ACS Photonics* 2021, 8, 738–744

Read Online

ACCESS | Metrics & More | Article Recommendations

ABSTRACT: Femtosecond laser fabrication outperforms the traditional fabrication techniques with high precision, high efficiency, low collateral damage and wide applicability, which has shown to be a powerful tool in precision machining. Imaging the ultrafast dynamics of femtosecond laser fabrication is necessary for understanding the processing mechanism and for establishing the corresponding physical models. Up to now, ultrafast measurement techniques based on the pump−probe strategy are the most used methods. However, they are limited by laser energy stability and materials surface uniformity, which have a heavy impact on the dynamic measurement precision of femtosecond laser fabrication. To overcome this limitation of the traditional pump−probe techniques, we developed chirped spectral mapping ultrafast photography (CSMUP), which can achieve single-shot real-time ultrafast imaging with a frame rate of about 250 billion frames per second (temporal frame interval of 4 ps) and a spatial resolution of less than 833 nm. We experimentally imaged the dynamics of femtosecond laser ablation in silicon under a 400 nm femtosecond laser exposure with CSMUP, and the experimental result agreed well with previous theoretical models. CSMUP provides a new strategy to improve the efficiency and accuracy of femtosecond laser fabrication by a single-shot dynamic measurement of the interaction between the femtosecond laser and materials, and it is expected to work as a real-time detection method for various ultrafast phenomena.

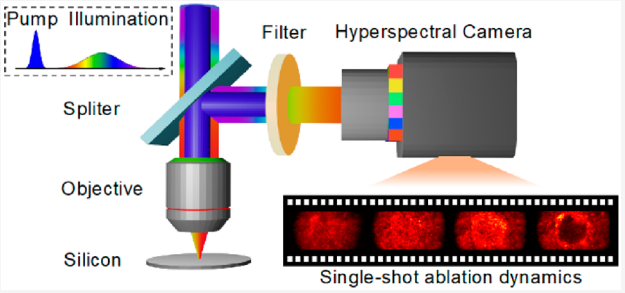

KEYWORDS: *ultrafast optical imaging, femtosecond laser fabrication, laser ablation, hyperspectral camera, chirped laser pulse*

Femtosecond laser fabrication has been widely applied in various materials processing, including metals,[1−3] semiconductors,[4−6] glasses,[7,8] polymers,[9,10] and so on. Compared with traditional fabrication techniques, such as mechanical processing,[11] chemical etching,[12] and ultrasonic machining,[13] femtosecond laser fabrication has the advantage of high precision, high efficiency, low collateral damage, and wide applicability for various materials. On the one hand, femtosecond laser fabrication has superior performance than the traditional fabrication in cutting, welding, drilling, and engraving with higher precision and efficiency. On the other hand, femtosecond laser fabrication can achieve novel materials modification, such as waveguide fabrication in glass,[14] black and colored materials surface,[15−17] materials with strong hydrophobicity,[18,19] hydrophilicity,[20,21] and surface modification of biocompatible materials.[22] Although femtosecond laser fabrication has been widely utilized in many fields, the mechanisms during the fabrication process are still not totally clear. Therefore, it is necessary to spatially and temporally measure the dynamics of femtosecond laser fabrication and understand the physical model in this process, which is helpful to further improve the efficiency and accuracy of femtosecond laser fabrication and extend its application fields. Up to now, many techniques have been developed to study the dynamics of femtosecond laser fabrication. For example, Sabbah et al. have studied the ultrafast optical response of silicon with a pump−probe reflectivity technique and obtained the quantitative information on carrier momentum relaxation, electron−phonon energy relaxation, and surface-mediated electron−hole recombination.[23] Mao et al. have studied femtosecond laser-induced plasma dynamics in a glass with time-resolved pump−probe shadowgraph.[24] Martin et al. have studied the laser-induced carrier trapping dynamics in wide-bandgap crystals with time-resolved spectral interferometry.[25] Hayasaki et al. have employed an interferometric time-resolved imaging method to observe the generation of carriers, thermal expansion, generation and propagation of shockwaves, and

Received: January 8, 2021
Published: February 23, 2021

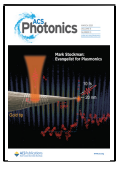

https://dx.doi.org/10.1021/acsphotonics.1c00043
ACS Photonics 2021, 8, 738−744

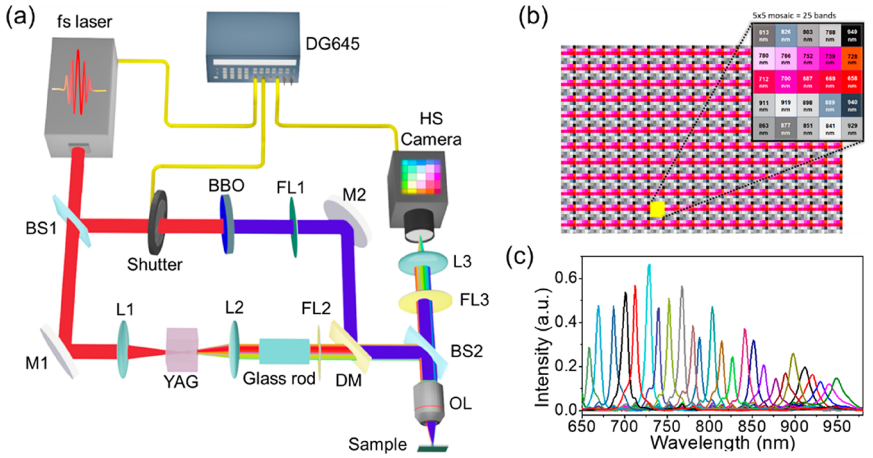

Figure 1. (a) System configuration of CSMUP for the femtosecond laser ablation measurement; (b) Filter arrangement on the CMOS sensor in the hyperspectral camera; (c) Spectral responses of 25 bands in the hyperspectral camera.

formation of refractive index changes in inside borosilicate glass.[26] Amer et al. have studied the shock wave generation on a polycrystalline boron nitride ceramic with pulsed digital holographic interferometry.[27] Jia et al. have studied the dynamics of femtosecond laser-induced periodic surface structures on silicon by using collinear pump−probe imaging.[28]

The traditional pump−probe-based ultrafast measurement techniques, such as the pump−probe microscopy and pump−probe shadowgraphy, can provide a high temporal resolution on the femtosecond scale, which depend on the laser pulse duration and pump−probe delay precision. Generally, these techniques are limited to measure the repeatable ultrafast phenomena. Obviously, it is not suitable for imaging the destructive and random processes, such as femtosecond laser ablation. To obtain the dynamics of these unrepeatable phenomena by the pump−probe method, the transient information with different pump−probe delays is separately collected at different position to retrieve the information on the time-resolved ultrafast process. However, considering the nonuniformity of material compositions, uneven morphology of surface, and instability of laser energy, the accuracy and reliability of this pump−probe technique cannot be guaranteed. Therefore, a single-shot ultrafast imaging technique is preferred for an unrepeatable dynamic measurement.

To overcome the disadvantages of the pump−probe scheme in the dynamic measurement, we develop a novel chirped spectral mapping ultrafast photography (CSMUP) to capture the dynamics of femtosecond laser fabrication with single-shot scheme. In CSMUP, a chirped broadband laser pulse with temporal dispersion works as the illumination source to record the ultrafast dynamics, and a hyperspectral camera works as the detector to obtain the spectral and spatial information. CSMUP is different from sequentially timed all-optical mapping photography utilizing spectral filtering (SF-STAMP) in the detection section,[29−31] where a diffraction optical element combined with a band-pass filter are generally employed as the temporal and spectral mapping device. Based on the temporal-spectral mapping relation in the chirped laser pulse, we can restore the temporal and spatial dynamics according to the spectral images. In our CSMUP system, the frame rate is about 250 billion frames per second (temporal frame interval of 4 ps), the spatial resolution is less than 833 nm, the image pixel size is 217 × 409, and the sequence depth is 25, which is determined by the spectral band number of the hyperspectral camera. Compared with SF-STAMP, CSMUP features with the larger image size, the higher spatial resolution and the more compact configuration. Through CSMUP, we have successfully measured the dynamics of femtosecond laser ablation on silicon under a 400 nm femtosecond laser exposure, and the experimental result can well validate the previous theoretical model.

The CSMUP system configuration for the dynamic measurement of femtosecond laser ablation is shown in Figure 1a. A Ti:sapphire laser amplifier provides the laser pulses with center wavelength of 800 nm, pulse duration of about 50 fs and repetition rate of 100 Hz. The output laser is split into two paths, one passes through a BBO crystal to generate a 400 nm pump pulse. A 450 nm short-pass filter (FL1) is utilized to remove the residual 800 nm laser, and an electronic shutter is utilized to conduct the single exposure. The other path is focused into a YAG crystal to generate a supercontinuum laser pulse with the broad spectral components ranged from visible (VIS) to near-infrared (NIR). A glass rod with a length of 60 cm is used to stretch the laser pulse width and generate a positively chirped supercontinuum laser pulse. A 650 nm long-pass filter (FL2) is used to remove the spectral components below 650 nm. The 400 nm pump pulse and chirped probe pulse are combined by a dichroic mirror (DM) and then focused on the surface of silicon with an objective lens (OL). The reflected signal pulse goes back to the same objective lens and then passes through a beamsplitter (BS2) and a lens (L3). A 650 nm long-pass filter (FL3) is used to block the 400 nm pump laser to prevent damage to the camera. The dynamic images are finally recorded with a hyperspectral camera (Ximea, MQ022HG-IM-SM5 × 5-NIR), which collects 25 spectral images of different wavelengths from 659 to 949 nm. Besides, a digital delay/pulse generator (Stanford Research Systems, DG645) is used to control the time delays among the hyperspectral camera trigger, electric shutter trigger and femtosecond laser trigger signal to achieve the single-shot exposure and image capture.

The hyperspectral camera is based on the standard CMOS sensors with hyperspectral Fabry−Perot interference filters that are added at the wafer-level on top of the pixel structure of the sensor. The sensors are designed to work in a specific spectral range, and these filters are added to any of the pixels of the sensor individually, as shown in Figure 1b. Here, this

https://dx.doi.org/10.1021/acsphotonics.1c00043
ACS Photonics 2021, 8, 738−744

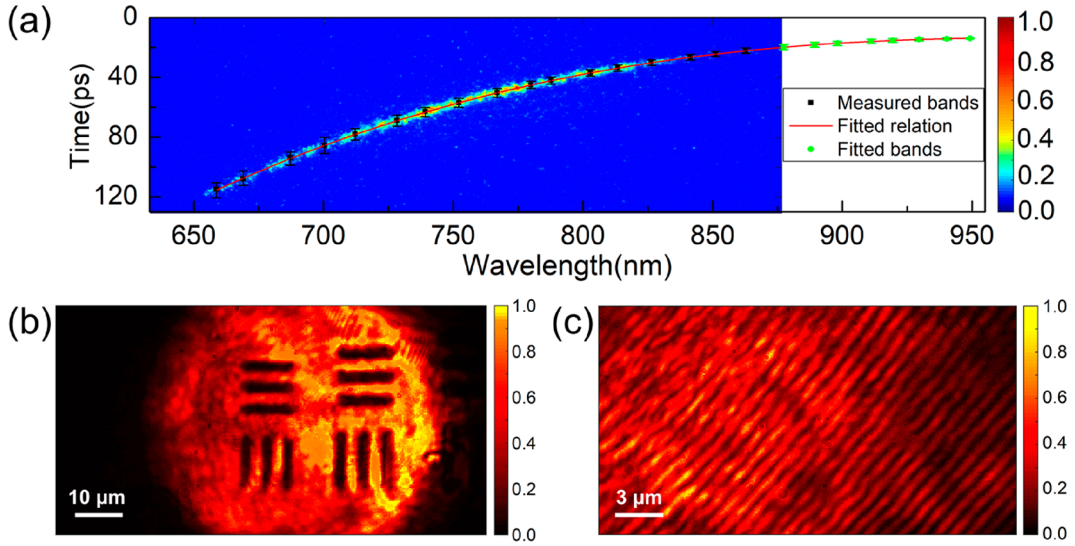

Figure 2. Temporal-spectral mapping of the chirped picosecond laser pulse measured by a streak camera combined with a spectrometer (a), together with the temporal and spectral positions of the spectral bands in the hyperspectral camera; Imaging of the 1951 USAF resolution target with 228 lp/mm (b) and a grating with 1200 lp/mm (c) measured by CSMUP.

hyperspectral camera has 25 individual spectral bands with an arrangement of 5 × 5, as shown in Figure 1c, and the total valid pixel size is 1085 × 2045. Thus, it can capture 25 hyperspectral images with 217 × 409 pixels in a single exposure.

In CSMUP, the direct measured result from the hyperspectral camera is a 2D image, which needs to be converted into a 3D dynamic scene (x−y−t) by afterward calculation. To describe the calculation process, the mathematical expression is given by

$$P(x', y', \lambda) = H_c H_p I(x, y) \tag{1}$$

where $I(x, y)$ is the raw 2D image from the hyperspectral camera; $P(x', y', \lambda)$ is 3D hyperspectral cube extracted from the raw 2D image; H_p is the band selection operator that rearranges the 2D data into 3D matrix according to the band distribution on the CMOS sensor; H_c is the coefficient correction operator that corrects the interactions between different band sensors, which can be written as

$$H_c = \sum_{x=1,y=1}^{n} C_{\lambda_x \lambda_y} \tag{2}$$

where n is the total number of spectral bands and C is the correction coefficient. The detailed parameters of H_p and H_c are provided, associated with the hyperspectral camera by manufacturer. Thus, the dynamic scene $S((x', y', t))$ can be expressed by

$$S(x', y', t) = MP(x', y', \lambda) \tag{3}$$

where M represents the spectral-temporal converting operator, which is decided by the temporal-spectral mapping of the chirped broadband laser pulse, and the different temporal positions are mapped to the corresponding spectral components. The temporal-spectral mapping is measured by a streak camera. Moreover, considering the intensity distribution of different spectral components, the spectral intensity normalization is also appended to the spectral-temporal converting operator M.

First, the temporal resolution of our CSMUP system was determined. Here, a streak camera (Hamamatsu, C7700) coupled with a spectrometer (Princeton Instruments, Acton SP2300) was used to measure the temporal-spectral mapping of the chirped laser pulse, and the experimental result is shown in Figure 2a. To facilitate the analysis, the temporal and spectral positions of these spectral bands in the hyperspectral camera are also given, together with the corresponding temporal width at each spectral band (error bar). Limited by the spectral response of the streak camera, the spectral components that are higher than 860 nm cannot be measured, and therefore, the temporal-spectral positions of these spectral bands are fitted (green dots). In our experiment, the whole duration width of the chirped laser pulse (i.e., the time window) is about 100 ps. The temporal-spectral mapping shows a slightly nonlinear character, which can be attributed to the high order dispersion of the glass rod. The time intervals between different spectral components are not the same because of the nonequidistant distribution of response bands in the hyperspectral camera and the nonlinear chirped character of the laser pulse. According to the temporal distribution of the chirped laser pulse (100 ps) and the spectral bands of the hyperspectral camera (25 bands), the frame rate was determined as about 250 billion frames per second, corresponding to the temporal frame interval of 4 ps. In addition, the time zero in the experiment was also determined with this streak camera. As can be seen, the temporal resolution of CSMUP depends on the chirped laser pulse duration, and therefore, it can be controlled by varying the chirped rate of the laser pulse.

Next, the spatial resolution of our CSMUP system was characterized. The static imaging of a 1951 USAF resolution test target (Thorlabs, R3L3S1N) with the minimum pattern of 228 lp/mm (line pairs per millimeter) was conducted by CSMUP with a 20× objective lens. Here, the resolution test target was illuminated with a chirped picosecond pulse with broadband spectra ranging from 650 to 975 nm, and the reflected signal was collected by the hyperspectral camera. A total of 25 bands of hyperspectral images were extracted from the hyperspectral data, which corresponded to a different time sequence. Since it was static imaging, these images were the same. Therefore, only the image with a spectral band of 803

https://dx.doi.org/10.1021/acsphotonics.1c00043
ACS Photonics 2021, 8, 738−744

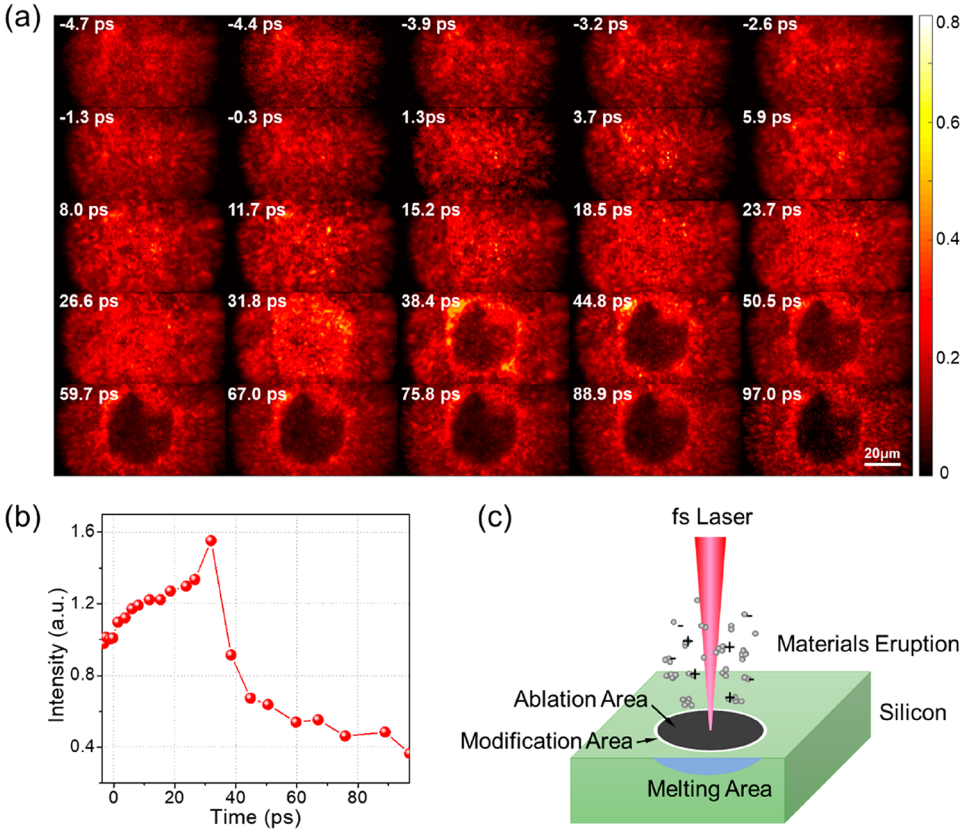

Figure 3. (a) Single-shot laser ablation dynamics measurement of silicon under a 400 nm femtosecond laser exposure captured by CSMUP (the image size is about 53 μm × 100 μm). (b) Time-dependent reflection intensity in the ablation area extracted from (a). (c) Schematic diagram of femtosecond laser ablation in silicon.

nm is presented in Figure 2b, which shows a clearly recognized pattern. Actually, these horizontal and vertical stripes in all the 25 images can be clearly observed. Besides, a 1200 lp/mm grating coated with gold was also captured by CSMUP with a 50× objective lens under the same experimental condition. Similarly, these grating lines can be well displayed in all the 25 images, and the representative image with the spectral band of 803 nm is shown in Figure 2c. The experimental observation shows that our CSMUP system has a spatial resolution of less than 833 nm. Generally, employing a higher NA objective lens can obtain a higher spatial resolution of CSMUP. However, higher NA typically implies higher magnification, and the ratio between NA and magnification is smaller; therefore, the image brightness is also lower. In addition, considering the lower quantum efficiency of the hyperspectral camera, this would result in the poor spectral image quality, that is, low signal-to-noise ratio (SNR), which would make the ultrafast dynamics difficult to be recognized. Therefore, here we did not utilize a higher 100× objective lens to further improve the spatial resolution of CSMUP. It is worth mentioning that there is no obvious difference in the static images of different spectral bands for the resolution test target and gating, which means that the wavelength dispersion has little effect on CSMUP.

To study the dynamics of femtosecond laser ablation, a 400 nm femtosecond laser pulse was used to induce the ablation on the polished silicon (100) wafer with a thickness of 0.5 mm, and CSMUP was utilized to record the ultrafast dynamics. In our experimental condition, the pump energy fluence was about 2.4 J/cm^2, which was higher than the single-shot ablation threshold of silicon (0.63 J/cm^2) reported in previous work.[32] Besides, limited by the pulse duration of the illumination laser, the ablation dynamics within 97 ps after the femtosecond laser excitation was recorded in our experiment, and the main early stage process of ablation were contained in the time window.

The single-shot laser ablation dynamics of silicon under a 400 nm femtosecond laser exposure captured by CSMUP is shown in Figure 3a, and the time-dependent reflection intensity in the ablation area is also extracted from Figure 3a, as shown in Figure 3b. Furthermore, to more intuitively illustrate the physical model of femtosecond laser fabrication, the schematic diagram of femtosecond laser ablation in silicon is given in Figure 3c. As can be seen, the reflection intensity of the illuminated area is slightly increased in the time of 1.3 ps, which is attributed to the increase of electron density. When the femtosecond laser pulse hits the silicon surface, the valence electrons in the silicon are excited to the conduction band by single-photon and multiphoton absorptions with phonon assistance. These free carriers obtain more energies by absorbing more photons. Besides, the impact ionization occurs under the high electric field of femtosecond laser and therefore increases the number density of free carriers. The electron density affects the dielectric constant of excited materials due to three effects: the state and band filling, the renormalization of the band structure and the free-carrier response, which finally determines the reflection rate.[33−35] After excitation, the electrons and holes are redistributed by the carrier−carrier and carrier−phonon scattering. The carrier−carrier scattering leads to the dephasing in the time of less than 10 fs, but the carrier distribution approaches a Fermi−Dirac distribution in hundreds of femtoseconds. The carrier−phonon scattering

https://dx.doi.org/10.1021/acsphotonics.1c00043
ACS Photonics 2021, 8, 738−744

leads to the energy transformation from the carriers to lattice, and the typical time scale for the corresponding lattice heating is in the range of a few tens of picoseconds before the carriers and lattice reach thermal equilibrium,[36] which can be well described with the two-temperature model.[37] From the time of 8 to 26.6 ps, the gradual increase of reflection intensity is observed, which is attributed to the lattice heating by the carrier−phonon scattering. The lattice heating will lead to the melt of Si, and the molten phase can be characterized by a metal-like state, featuring a high reflectivity. During this process, a melting front propagates from the surface into the material with a velocity limited by the speed of sound.[38,39] In the time of 31.8 ps, the reflection intensity increases significantly. When the temperature is higher than the boiling temperature, the liquid is superheated to approach the thermodynamic equilibrium critical temperature. Then, the phase explosion occurs with the materials removed from the silicon surface associated with evaporation and explosive boiling.[40] As can be seen in the time of 38.4 ps, the center area becomes dark, which means the materials eruption has started. The darkening is attributed to the surface morphology change induced by the materials eruption and the light absorption/scattering induced by the vaporised material. Besides, the surrounding area becomes bright, which verifies the surface melting without material eruption due to the laser excitation intensity below the ablation threshold.[41,42] For the time scale from 38.4 to 97 ps, the center area becomes darker, but the shape of the ablation area keeps unchanged, which indicates that the emission can last more than 97 ps, such a process has been proved that the material eruption can last up to the scale of microseconds,[43] and the ablation occurs with the energy density being higher than critical threshold.[44] Generally, the ablation dynamics of silicon under a 400 nm femtosecond laser exposure captured by CSMUP is in accordance with previous works.

Similarly, CSMUP can also be used to record other femtosecond laser fabrication processes to reveal the underlying the physical mechanism, such as femtosecond laser cutting,[45] welding,[46] and drilling.[47] Because of featuring the inherent single-shot character, CSMUP can gather the temporal and spatial dynamic information in a single shot without renewing the action area during the measurement for the unrepeatable process. Besides, CSMUP is based on a commercial hyperspectral camera instead of expensive and customized devices (such as streak camera) in some single-shot ultrafast imaging systems,[48,49] and so it is more economical and flexible. Nonetheless, there are still some limitations for CSMUP. For example, the unequal temporal frame intervals in CSMUP may cause some difficulties in the dynamic analysis; CSMUP has the lower spatial resolution due to the mosaic arrangement of spectral filters in the image sensor; CSMUP is unsuitable for the measurement of the spectral-sensitive dynamic scene because of the spectral-temporal cross-talk.

In conclusion, we have developed a novel CSMUP technique to realize single-shot real-time ultrafast imaging of laser ablation on silicon under a 400 nm femtosecond laser exposure, and demonstrated that the measured dynamics of femtosecond laser ablation can well validate previous theoretical models. CSMUP has shown to be a well-established tool to study the unrepeatable phenomenon, which overcomes the shortcomings of low stability and accuracy in the traditional pump−probe based photography. With the variable chirped laser pulse, CSMUP can work in tunable time windows, which can be applied in recording various ultrafast fabrication processes, such as the laser-induced period surface structure on metals and semiconductors,[50,51] the femtosecond laser-induced nanogratings inside a glass,[52] the bubble formation,[53] and so on. Integrating with other imaging systems, CSMUP can also be expended in more areas for unrepeatable phenomena without the limitation in ultrafast laser fabrication, for example, three-dimensional imaging[54] and ultrafast holography.[55]

AUTHOR INFORMATION

Corresponding Authors

Dalong Qi − *State Key Laboratory of Precision Spectroscopy, School of Physics and Electronic Science, East China Normal University, Shanghai 200062, China*; Email: dlqi@lps.ecnu.edu.cn

Feng Huang − *School of Mechanical Engineering and Automation, Fuzhou University, Fuzhou 350000, China*; Email: huangf@fzu.edu.cn

Shian Zhang − *State Key Laboratory of Precision Spectroscopy, School of Physics and Electronic Science, East China Normal University, Shanghai 200062, China; Collaborative Innovation Center of Extreme Optics, Shanxi University, Taiyuan 030006, China; Collaborative Innovation Center of Light Manipulations and Applications, Shandong Normal University, Jinan 250358, China*; orcid.org/0000-0003-3168-4962; Email: sazhang@phy.ecnu.edu.cn

Authors

Yunhua Yao − *State Key Laboratory of Precision Spectroscopy, School of Physics and Electronic Science, East China Normal University, Shanghai 200062, China*; orcid.org/0000-0002-1894-1867

Yilin He − *State Key Laboratory of Precision Spectroscopy, School of Physics and Electronic Science, East China Normal University, Shanghai 200062, China*

Fengyan Cao − *State Key Laboratory of Precision Spectroscopy, School of Physics and Electronic Science, East China Normal University, Shanghai 200062, China*

Jiali Yao − *State Key Laboratory of Precision Spectroscopy, School of Physics and Electronic Science, East China Normal University, Shanghai 200062, China*

Pengpeng Ding − *State Key Laboratory of Precision Spectroscopy, School of Physics and Electronic Science, East China Normal University, Shanghai 200062, China*

Chengzhi Jin − *State Key Laboratory of Precision Spectroscopy, School of Physics and Electronic Science, East China Normal University, Shanghai 200062, China*

Xianyu Wu − *School of Mechanical Engineering and Automation, Fuzhou University, Fuzhou 350000, China*

Lianzhong Deng − *State Key Laboratory of Precision Spectroscopy, School of Physics and Electronic Science, East China Normal University, Shanghai 200062, China*

Tianqing Jia − *State Key Laboratory of Precision Spectroscopy, School of Physics and Electronic Science, East China Normal University, Shanghai 200062, China*

Jinyang Liang − *Laboratory of Applied Computational Imaging, Centre Énergie Matériaux Télécommunications, Institut National de la Recherche Scientifique, Varennes, Québec J3X1S2, Canada*

https://dx.doi.org/10.1021/acsphotonics.1c00043
ACS Photonics 2021, 8, 738−744

Zhenrong Sun − *State Key Laboratory of Precision Spectroscopy, School of Physics and Electronic Science, East China Normal University, Shanghai 200062, China*

Complete contact information is available at: https://pubs.acs.org/10.1021/acsphotonics.1c00043

Author Contributions

#These authors contributed equally to this work.

Notes

The authors declare no competing financial interest.

■ ACKNOWLEDGMENTS

This work was partially supported by the National Natural Science Foundation of China (Grant Nos. 91850202, 11774094, 11727810, 11804097, and 12074121) and the Science and Technology Commission of Shanghai Municipality (Grant Nos. 19560710300 and 20ZR1417100).

■ REFERENCES

(1) Vorobyev, A. Y.; Guo, C. Enhanced absorptance of gold following multipulse femtosecond laser ablation. *Phys. Rev. B: Condens. Matter Mater. Phys.* **2005**, *72*, 195422.
(2) Vorobyev, A. Y.; Guo, C. L. Femtosecond laser nanostructuring of metals. *Opt. Express* **2006**, *14*, 2164−2169.
(3) Leitz, K.; Redlingshöfer, B.; Reg, Y.; Otto, A.; Schmidt, M. Metal Ablation with Short and Ultrashort Laser Pulses. *Phys. Procedia* **2011**, *12*, 230−238.
(4) Borowiec, A.; Haugen, H. K. Subwavelength ripple formation on the surfaces of compound semiconductors irradiated with femtosecond laser pulses. *Appl. Phys. Lett.* **2003**, *82*, 4462−4464.
(5) Sundaram, S. K.; Mazur, E. Inducing and probing non-thermal transitions in semiconductors using femtosecond laser pulses. *Nat. Mater.* **2002**, *1*, 217−224.
(6) Pan, C.; Wang, Q.; Sun, J.; Wang, F.; Sun, J.; Wang, G.; Lu, Y.; Jiang, L. Dynamics and its modulation of laser-induced plasma and shockwave in femtosecond double-pulse ablation of silicon. *Appl. Phys. Express* **2020**, *13*, 12006.
(7) Hnatovsky, C.; Taylor, R. S.; Rajeev, P. P.; Simova, E.; Bhardwaj, V. R.; Rayner, D. M.; Corkum, P. B. Pulse duration dependence of femtosecond-laser-fabricated nanogratings in fused silica. *Appl. Phys. Lett.* **2005**, *87*, 14104.
(8) Streltsov, A. M.; Borrelli, N. F. Fabrication and analysis of a directional coupler written in glass by nanojoule femtosecond laser pulses. *Opt. Lett.* **2001**, *26*, 42.
(9) Suriano, R.; Kuznetsov, A.; Eaton, S. M.; Kiyan, R.; Cerullo, G.; Osellame, R.; Chichkov, B. N.; Levi, M.; Turri, S. Femtosecond laser ablation of polymeric substrates for the fabrication of microfluidic channels. *Appl. Surf. Sci.* **2011**, *257*, 6243−6250.
(10) Rebollar, E.; Vázquez De Aldana, J. R.; Pérez-Hernández, J. A.; Ezquerra, T. A.; Moreno, P.; Castillejo, M. Ultraviolet and infrared femtosecond laser induced periodic surface structures on thin polymer films. *Appl. Phys. Lett.* **2012**, *100*, 41106.
(11) Liu, D.; Tang, Y.; Cong, W. L. A review of mechanical drilling for composite laminates. *Compos. Struct.* **2012**, *94*, 1265−1279.
(12) Qian, B.; Shen, Z. Fabrication of Superhydrophobic Surfaces by Dislocation-Selective Chemical Etching on Aluminum, Copper, and Zinc Substrates. *Langmuir* **2005**, *21*, 9007−9009.
(13) Thoe, T. B.; Aspinwall, D. K.; Wise, M. L. H. Review on ultrasonic machining. *Int. J. Mach. Tools Manufact.* **1998**, *38*, 239−255.
(14) Chan, J. W.; Huser, T. R.; Risbud, S. H.; Krol, D. M. Modification of the fused silica glass network associated with waveguide fabrication using femtosecond laser pulses. *Appl. Phys. A: Mater. Sci. Process.* **2003**, *76*, 367−372.
(15) Wu, C.; Crouch, C. H.; Zhao, L.; Carey, J. E.; Younkin, R.; Levinson, J. A.; Mazur, E.; Farrell, R. M.; Gothoskar, P.; Karger, A. Near-unity below-band-gap absorption by microstructured silicon. *Appl. Phys. Lett.* **2001**, *78*, 1850−1852.
(16) Vorobyev, A. Y.; Guo, C. Spectral and polarization responses of femtosecond laser-induced periodic surface structures on metals. *J. Appl. Phys. (Melville, NY, U. S.)* **2008**, *103*, 43513.
(17) Vorobyev, A. Y.; Guo, C. Direct femtosecond laser surface nano/microstructuring and its applications. *Laser Photonics Rev.* **2013**, *7*, 385−407.
(18) Zorba, V.; Persano, L.; Pisignano, D.; Athanassiou, A.; Stratakis, E.; Cingolani, R.; Tzanetakis, P.; Fotakis, C. Making silicon hydrophobic: wettability control by two-lengthscale simultaneous patterning with femtosecond laser irradiation. *Nanotechnology* **2006**, *17*, 3234−3238.
(19) Barberoglou, M.; Zorba, V.; Stratakis, E.; Spanakis, E.; Tzanetakis, P.; Anastasiadis, S. H.; Fotakis, C. Bio-inspired water repellent surfaces produced by ultrafast laser structuring of silicon. *Appl. Surf. Sci.* **2009**, *255*, 5425−5429.
(20) Papadopoulou, E. L.; Barberoglou, M.; Zorba, V.; Manousaki, A.; Pagkozidis, A.; Stratakis, E.; Fotakis, C. Reversible Photoinduced Wettability Transition of Hierarchical ZnO Structures. *J. Phys. Chem. C* **2009**, *113*, 2891−2895.
(21) Vorobyev, A. Y.; Guo, C. Water sprints uphill on glass. *J. Appl. Phys. (Melville, NY, U. S.)* **2010**, *108*, 123512.
(22) Kurella, A.; Dahotre, N. B. Review paper: Surface Modification for Bioimplants: The Role of Laser Surface Engineering. *J. Biomater. Appl.* **2005**, *20*, 5−50.
(23) Sabbah, A. J.; Riffe, D. M. Femtosecond pump-probe reflectivity study of silicon carrier dynamics. *Phys. Rev. B: Condens. Matter Mater. Phys.* **2002**, *66*, 165217.
(24) Mao, X.; Mao, S. S.; Russo, R. E. Imaging femtosecond laser-induced electronic excitation in glass. *Appl. Phys. Lett.* **2003**, *82*, 697−699.
(25) Martin, P.; Guizard, S.; Daguzan, P.; Petite, G.; D'Oliveira, P.; Meynadier, P.; Perdrix, M. Subpicosecond study of carrier trapping dynamics in wide-band-gap crystals. *Phys. Rev. B: Condens. Matter Mater. Phys.* **1997**, *55*, 5799−5810.
(26) Hayasaki, Y.; Isaka, M.; Takita, A.; Juodkazis, S. Time-resolved interferometry of femtosecond-laser-induced processes under tight focusing and close-to-optical breakdown inside borosilicate glass. *Opt. Express* **2011**, *19*, 5725.
(27) Amer, E.; Gren, P.; Sjodahl, M. Shock wave generation in laser ablation studied using pulsed digital holographic interferometry. *J. Phys. D: Appl. Phys.* **2008**, *41*, 215502.
(28) Jia, X.; Jia, T. Q.; Peng, N. N.; Feng, D. H.; Zhang, S. A.; Sun, Z. R. Dynamics of femtosecond laser-induced periodic surface structures on silicon by high spatial and temporal resolution imaging. *J. Appl. Phys. (Melville, NY, U. S.)* **2014**, *115*, 143102.
(29) Nakagawa, K.; Iwasaki, A.; Oishi, Y.; Horisaki, R.; Tsukamoto, A.; Nakamura, A.; Hirosawa, K.; Liao, H.; Ushida, T.; Goda, K.; Kannari, F.; Sakuma, I. Sequentially timed all-optical mapping photography (STAMP). *Nat. Photonics* **2014**, *8*, 695−700.
(30) Suzuki, T.; Isa, F.; Fujii, L.; Hirosawa, K.; Nakagawa, K.; Goda, K.; Sakuma, I.; Kannari, F. Sequentially timed all-optical mapping photography (STAMP) utilizing spectral filtering. *Opt. Express* **2015**, *23*, 30512−30522.
(31) Suzuki, T.; Hida, R.; Yamaguchi, Y.; Nakagawa, K.; Saiki, T.; Kannari, F. Single-shot 25-frame burst imaging of ultrafast phase transition of $Ge_2Sb_2Te_5$ with a sub-picosecond resolution. *Appl. Phys. Express* **2017**, *10*, 92502.
(32) Lee, S.; Yang, D.; Nikumb, S. Femtosecond laser micromilling of Si wafers. *Appl. Surf. Sci.* **2008**, *254*, 2996−3005.
(33) Sokolowski-Tinten, K.; von der Linde, D. Generation of dense electron-hole plasmas in silicon. *Phys. Rev. B: Condens. Matter Mater. Phys.* **2000**, *61*, 2643.
(34) Shank, C. V.; Yen, R.; Hirlimann, C. Time-resolved reflectivity measurements of femtosecond-optical-pulse-induced phase transitions in silicon. *Phys. Rev. Lett.* **1983**, *50*, 454.
(35) Garcia-Lechuga, M.; Puerto, D.; Fuentes-Edfuf, Y.; Solis, J.; Siegel, J. Ultrafast moving-spot microscopy: Birth and growth of laser-

induced periodic surface structures. *ACS Photonics* **2016**, *3*, 1961−1967.
(36) Rethfeld, B.; Sokolowski-Tinten, K.; von der Linde, D.; Anisimov, S. I. Timescales in the response of materials to femtosecond laser excitation. *Appl. Phys. A: Mater. Sci. Process.* **2004**, *79*, 767−769.
(37) Taylor, L. L.; Scott, R. E.; Qiao, J. Integrating two-temperature and classical heat accumulation models to predict femtosecond laser processing of silicon. *Opt. Mater. Express* **2018**, *8*, 648.
(38) Rethfeld, B.; Ivanov, D. S.; Garcia, M. E.; Anisimov, S. I. Modelling ultrafast laser ablation. *J. Phys. D: Appl. Phys.* **2017**, *50*, 193001.
(39) Rethfeld, B.; Sokolowski-Tinten, K.; von der Linde, D.; Anisimov, S. I. Ultrafast thermal melting of laser-excited solids by homogeneous nucleation. *Phys. Rev. B: Condens. Matter Mater. Phys.* **2002**, *65*, 092103.
(40) Chen, J. K.; Beraun, J. E. Modelling of ultrashort laser ablation of gold films in vacuum. *J. Opt. A: Pure Appl. Opt.* **2003**, *5*, 168−173.
(41) Downer, M. C.; Fork, R. L.; Shank, C. V. Femtosecond imaging of melting and evaporation at a photoexcited silicon surface. *J. Opt. Soc. Am. B* **1985**, *2*, 595−599.
(42) Siegel, J.; Puerto, D.; Gawelda, W.; Bachelier, G.; Solis, J.; Ehrentraut, L.; Bonse, J. Plasma formation and structural modification below the visible ablation threshold in fused silica upon femtosecond laser irradiation. *Appl. Phys. Lett.* **2007**, *91*, 82902.
(43) Koch, J.; Heiroth, S.; Lippert, T.; Günther, D. Femtosecond laser ablation: Visualization of the aerosol formation process by light scattering and shadowgraphic imaging. *Spectrochim. Acta, Part B* **2010**, *65*, 943−949.
(44) Bonse, J.; Baudach, S.; Krüger, J.; Kautek, W.; Lenzner, M. Femtosecond laser ablation of silicon-modification thresholds and morphology. *Appl. Phys. A: Mater. Sci. Process.* **2002**, *74*, 19−25.
(45) Bärsch, N.; Körber, K.; Ostendorf, A.; Tönshoff, K. H. Ablation and cutting of planar silicon devices using femtosecond laser pulses. *Appl. Phys. A: Mater. Sci. Process.* **2003**, *77*, 237−242.
(46) Hélie, D.; Bégin, M.; Lacroix, F.; Vallée, R. Reinforced direct bonding of optical materials by femtosecond laser welding. *Appl. Opt.* **2012**, *51*, 2098.
(47) Ahn, S.; Hwang, D. J.; Park, H. K.; Grigoropoulos, C. P. Femtosecond laser drilling of crystalline and multicrystalline silicon for advanced solar cell fabrication. *Appl. Phys. A: Mater. Sci. Process.* **2012**, *108*, 113−120.
(48) Liang, J.; Wang, L. V. Single-shot ultrafast optical imaging. *Optica* **2018**, *5*, 1113−1127.
(49) Qi, D.; Zhang, S.; Yang, C.; He, Y.; Cao, F.; Yao, J.; Ding, P.; Gao, L.; Jia, T.; Liang, J.; Sun, Z.; Wang, L. V. Single-shot compressed ultrafast photography: a review. *Adv. Photonics* **2020**, *2*, 14003.
(50) Bonse, J.; Krüger, J.; Höhm, S.; Rosenfeld, A. Femtosecond laser-induced periodic surface structures. *J. Laser Appl.* **2012**, *24*, 42006.
(51) Liu, J.; Zhao, H.; Cheng, K.; Ju, J.; Feng, D.; Zhang, S.; Sun, Z.; Jia, T. Ultrafast dynamics of the thin surface plasma layer and the periodic ripples formation on GaP crystal irradiated by a single femtosecond laser pulse. *Opt. Express* **2019**, *27*, 37859−37876.
(52) Zhang, B.; Liu, X.; Qiu, J. Single femtosecond laser beam induced nanogratings in transparent media-Mechanisms and applications. *J. Materiomics* **2019**, *5*, 1−14.
(53) Vogel, A.; Linz, N.; Freidank, S.; Paltauf, G. Femtosecond-laser-induced nanocavitation in water: implications for optical breakdown threshold and cell surgery. *Phys. Rev. Lett.* **2008**, *100*, 38102.
(54) Okoshi, T. *Three-Dimensional Imaging Techniques*; Academic Press: New York, 1976 DOI: 10.1016/B978-0-12-525250-8.50002-5.
(55) Tikan, A.; Bielawski, S.; Szwaj, C.; Randoux, S.; Suret, P. Single-shot measurement of phase and amplitude by using a heterodyne time-lens system and ultrafast digital time-holography. *Nat. Photonics* **2018**, *12*, 228−234.

https://dx.doi.org/10.1021/acsphotonics.1c00043
ACS Photonics 2021, 8, 738−744